Journal of Cerebral Blood Flow & Metabolism (2015) 35, 20–27

www.jcbfm.com

RAPID COMMUNICATION

Regional distribution of selective neuronal loss and microglial activation across the MCA territory after transient focal ischemia: quantitative versus semiquantitative systematic immunohistochemical assessment

Julius V Emmrich[1,2,6], Sohail Ejaz[1,6], Jonas J Neher[3,7], David J Williamson[1,4] and Jean-Claude Baron[1,5]

Histopathologic assessment in transient middle cerebral artery occlusion (MCAo) rodent models generally lacks comprehensiveness and exposes to interobserver bias. Here we compared a novel quantitative assessment of regional infarction, selective neuronal loss (SNL) and microglial activation (MA) across the MCA territory to a previously published semiquantitative visual protocol. NeuN and OX42 immunohistochemistry was applied after either 15 or 45 minutes distal MCAo to maximize SNL and infarction, respectively. Survival times varied from 28 to 60 days to cover potential biases such as delayed tissue shrinkage. Damage was assessed using a template of 44 cytoarchitectonic regions of interest (ROIs) mapped onto a subset of digitized coronal sections spanning the MCA territory. For each ROI were obtained a semiquantitative visually determined index of histopathologic changes (method 1), and Ipsilateral/contralesional ratios of remaining neurons and activated microglia cell counts (method 2). There was excellent agreement between the two methods for 28-day survival for both MCAo durations, whereas method 2 more sensitively detected subtle SNL and MA at 45 days and 60 days after 15-minute MCAo. Thus the visual method is accurate for usual degrees of ischemic damage, but absolute cell quantification is superior to detect subtle changes and should therefore be preferred in brief MCAo models, although requires optimal staining quality.

Journal of Cerebral Blood Flow & Metabolism (2015) **35,** 20–27; doi:10.1038/jcbfm.2014.181; published online 29 October 2014

Keywords: brain ischemia; immunohistochemistry; inflammation; selective neuronal death

INTRODUCTION

Within the acutely ischemic brain, there are two major regions of injury: the ischemic core, where severe hypoperfusion rapidly causes irreversible membrane damage, cell death, and progression toward tissue infarction (pan-necrosis), and the comparatively less hypoperfused ischemic penumbra, where cells are equally nonfunctional but are still viable and that will escape infarction if perfusion is reestablished early enough.[1,2] Although rescuing the penumbra is the main determinant of neurological recovery, studies in humans and various animal species have shown that the salvaged penumbra may be affected by selective neuronal loss (SNL). Importantly, SNL, which refers to the death of single or patches of neurons with preserved tissue integrity, is consistently associated with microglial activation (MA) in the first few weeks after injury.[3] As both these processes might impede functional recovery after reperfusion, they are considered potential new therapeutic targets in postacute ischemic stroke (see Baron[4] for review). It is therefore important in animal models of transient focal cerebral ischemia mimicking early recanalization in the clinical setting to be able to reliably assess the regional distribution and intensity of the full spectrum of tissue damage, from pan-necrosis to subtle SNL and MA.

Histopathologic evidence of SNL and MA within the rescued penumbra has been well characterized in various animal models of focal ischemia. As recently extensively reviewed,[3] transient (⩽30 minutes) proximal middle cerebral artery occlusion (tMCAo) in rats causes mainly striatal SNL with small and occasional cortical patches of SNL. However, cortical pathology is of particular clinical relevance owing to its greater rescueability by thrombolysis and more pronounced and long-lasting behavioral effects in the clinical setting (see Baron[4] for review), which also applies to sensorimotor function in rodent models.[3,5–7] Consistently extensive, pure cortical SNL can be induced using distal tMCAo.[8–10]

Hematein and eosin and Nissl staining have been traditionally used for postmortem assessment of SNL, detecting dead or dying

[1]Department of Clinical Neurosciences, Stroke Research Group, University of Cambridge, Cambridge, UK; [2]Department of Neurology, Charité—Universitätsmedizin Berlin, Berlin, Germany; [3]Department of Biochemistry, University of Cambridge, Cambridge, UK; [4]Department of Clinical Neurosciences, Wolfson Brain Imaging Centre, University of Cambridge, Cambridge, UK and [5]INSERM U894, Hôpital Sainte-Anne, Université Paris Descartes/Sorbonne Paris Cité, Paris, France. Correspondence: Professor J-C Baron, INSERM U894, 2 ter rue d'Alésia, Paris 75014, France.
E-mail: jean-claude.baron@inserm.fr
This study was funded by an EU Grant (EUSTROKE Health-F2-2008-2022131); JVE was funded by a grant from Theracur Stiftung; DJW was funded by an MRC collaborative grant (G0600986).
[6]These authors contributed equally to this work.
[7]Present address: Department of Cellular Neurology, Hertie Institute for Clinical Brain Research, University of Tübingen, Tübingen, Germany.
Received 1 August 2014; revised 10 September 2014; accepted 30 September 2014; published online 29 October 2014

neurons based on evaluation of cellular morphology and staining features.[11–13] However, a limitation of these conventional staining methods is that once dead neurons have been cleared by phagocytosis, neuronal loss can be difficult to assess on the background of similarly stained glial cells or neuropil, potentially leading to underestimating or even completely missing the damage. In addition, quantitative assessment of MA using these nonspecific stains is not practical. In contrast, thanks to the more recent introduction of specific antibodies directed against neuronal or microglial cellular surface markers such as NeuN or OX42, respectively, straightforward assessment of SNL and MA, expressed as reduced or increased staining intensity against background, respectively, is now possible. In addition, selective immunohistochemical staining allows for easy quantification of these changes by standard cell-counting methodology.

So far, various approaches to immunohistochemical evaluation of SNL or MA have been proposed. Most commonly, for time constraint reasons analysis is conducted in a noncomprehensive manner, i.e., counting neurons or microglial cells per randomly selected nonoverlapping microscopic fields.[11–13] Another approach involves visual scoring on small number of prespecified brain regions.[8,14,15] However, both methods lack comprehensiveness and expose to the risk of interobserver bias, especially given the well-established intersubject variability in extent and severity of ischemic damage, and the fact that SNL can occur in cortical areas remote from the ischemic core.[3] Although a comprehensive and systematic assessment of the whole brain avoids these issues, it can be extremely time-consuming unless specific solutions are implemented. One recently proposed and validated solution involves the visual scoring of a fixed template of cytoarchitectonically defined regions of interest (ROIs) spanning the MCA territory.[10] Yet, visual methods only allow for a semiquantitative assessment using arbitrary scales to grade the severity and/or extent of changes. In addition, visual assessment might miss subtle yet meaningful changes. Although quantitative cell counting does not have these potential limitations, systematic MCA territory assessment has not been reported so far.

The aim of the present study therefore was to compare and assess the respective merits of two distinct methods to assess ischemic brain damage across separate ROIs spanning the MCA territory, namely the above visual scoring method[10] and a novel software-assisted automated quantitative cell-counting method. To allow a meaningful comparison, the same template of ROIs was used in both methods. Furthermore, to encompass the entire spectrum of ischemic damage subtypes, we used both a relatively long tMCAo model, namely 45 minutes, where infarction is known to frequently occur[9] as well as a much shorter duration, namely 15 minutes, where only SNL is expected.[3] In both cases, we used the distal clip tMCAo method to maximize on cortical pathology. In addition, to assess the most subtle end of the spectrum of ischemia-induced changes, we studied a sample of rats with very long survival after 15-minute tMCAo, namely 45 and 60 days, where inflammation is expected to have become minimal or even absent,[3] while neuronal loss may become difficult to measure because of late tissue shrinkage[16,17] and/or neurogenesis.[18] To compare the two methods, we performed correlation analyses between the visual scores for SNL/MA and the cell counts for neurons and microglia for each ROI across groups.

MATERIALS AND METHODS

Animals

All experiments were performed in accordance with the UK Animals (Scientific Procedures) Act (1986) and were approved by the University of Cambridge Ethical Review Panel. According to this approval, the number of subjects was limited to the minimum required to obtain scientifically meaningful results. Twenty male spontaneously hypertensive rats, 10 to 12 weeks of age, were used for surgical induction of ischemia. We chose to use this strain because it has been shown to result in the most consistent as well as extensive cortical ischemia after distal MCAo.[19,20] This manuscript was written up according to the Animal Research: Reporting of *In Vivo* Experiments (ARRIVE) guidelines for reporting animal experiments.

Anesthesia

All animals were induced with 4% isoflurane plus oxygen and nitrous oxide (ratio 0.3/0.7) and maintained with 2% isoflurane during surgical procedures. Temperature was maintained at 37°C throughout the surgery using a heating blanket.

Temporary Middle Cerebral Artery Occlusion

Rats were subjected to 15 minutes ($n = 12$) or 45 minutes ($n = 8$) distal clip tMCAo, and survived for 28 ($n = 14$; 6 and 8 in each tMCAo group, respectively), 45 ($n = 3$; all 15 minutes tMCAo), or 60 days ($n = 3$; 15 minutes tMCAo). Findings in the subgroup of rats subjected to 45 minutes tMCAO have already been published in part elsewhere.[9] The distal clip tMCAo model was performed using Buchan *et al*'s method[19] as implemented in our laboratory.[9,10,21] Briefly, the left common carotid artery was isolated through a ventral midline incision on the neck and a loose ligature of 4-0 silk suture was placed around it. With the rat positioned onto its right flank, a 2.5 cm skin incision perpendicular to, and bisecting the line between the lateral canthus of the right eye and the external auditory canal was made, and the underlying temporalis muscle excised to reveal the base of the skull. Under direct visualization, the underlying temporalis muscle was excised and craniectomy was performed under saline irrigation to expose the left MCA through a 2-mm burr hole drilled 2 to 3 mm rostral to the fusion of the zygomatic arch with the squamosal bone. The dura was retracted to visualize the MCA at a position where it crosses the inferior cerebral vein, which lies within the rhinal fissure. A micro-aneurysm clip (No 1, Codman, Sundt AVM, Raynham, MA, USA) was placed on the MCA proximal to the point where it crosses the inferior cerebral vein, and the left common carotid artery was permanently ligated. The clip was removed after 15 or 45 minutes and the wound was closed after visual verification of the restoration of blood flow.[10] The effects on tissue perfusion of distal ligation as performed in our laboratory have been published previously.[10]

Cryosectioning

The experiment was terminated by perfusion-fixation through the heart as detailed elsewhere.[10] The whole brain was embedded in optimal cutting temperature medium and mounted on a specimen holder of a freezing sledge microtome for serial 40 μm coronal sections. Sections were collected from across the MCA territory, i.e. from the level of the forceps minor of the corpus callosum to the visual cortex and the superior colliculi (bregma 3.7 to -6.80 mm)[10] and mounted on gelatine-coated slides.

Immunohistochemistry and Image Acquisition

For immunohistochemistry, frozen brain sections were quenched with 10% methanol and 10% H_2O_2 for 5 minutes and blocked in 3% normal horse serum (S-2000, Vector Laboratories, Burlingame, CA, USA) in phosphate-buffered saline. Consecutive sections were incubated overnight at 4°C with primary antibody specific for nuclear protein for mature neurons (NeuN, 1:1000; MAB377, Chemicon International, Temecula, CA, USA) and reactive microglia and macrophages (OX42, 1:400; MCA275R, Serotec, Kidlington, UK). After washing three times with Tris-buffered saline, sections were incubated with biotinylated antimouse IgG (rat-absorbed: dilution 1:200; Vector Laboratories) secondary antibodies, washed with Tris-buffered saline, incubated in avidin–biotin horseradish peroxidase complex solution (ABC Kit, Vector Laboratories) for 10 minutes, and the reaction product visualized with diaminobenzidine (DAB kit, Vector Laboratories). Finally, the sections were dehydrated through alcohol, cleared with xylene and slides were cover-slipped with di-n-butyle phthalate in xylene mounting medium (1330-20-7, Merck, White House Station, NJ, USA).

Eight coronal sections spanning the cortical MCA territory were selected for analysis at the following locations relative to the bregma: 2.70, 1.00, -0.26, -0.92, -2.12, -3.14, -4.52, and -6.04 mm.[9,10] Stained sections were captured via whole-slide scanning on a NanoZoomer slide scanner (Hamamatsu Photonics, Hamamatsu City, Japan) and exported with NDP viewer software (Hamamatsu Photonics). Composite images were stitched automatically from individual frames.

Image Processing

A set of symmetrical anatomic cytoarchitectonic ROIs derived from the stereotaxic atlas of the rat brain (Paxinos & Watson, 2004) was applied to each digitized section, as described previously.[9,10] Per hemisphere, the ROI template is composed of 39 cytoarchitectonically distinct cortical ROIs, 4 caudate/putamen ROIs and 1 thalamus ROI. The resulting digitized maps of individual animals at corresponding coronal levels were then mapped into the common 44-ROI template using Adobe Photoshop CS (Adobe Systems, Mountain View, CA, USA) and digital images of each section with the superimposed ROIs were acquired (Figure 1A).

Visual Scoring

Briefly, two experienced scorers independently rated OX42 pathology in each ROI of each section and each animal, using a visual grading scale integrating pathology across the ROI. This scale comprises both a severity score (0 to 10; 0 = normal OX42 staining relative to homologous ROI on unaffected side, 10 = maximally increased OX42 staining, i.e., densely packed, darkly stained cells; with 1 to 9 being intermediate; not considering the actual shape of the cells, i.e., ramified versus ameboid) and an area score (0 to 10; 0 = no abnormally increased OX42 staining in any part of the ROI, 10 = whole ROI affected by abnormally increased OX42 staining, with 1 to 9 being intermediate extent relative to the corresponding contralateral ROI). For each ROI, the area score was then multiplied by the severity score, to yield an overall OX42 score expressing both the extent and degree of abnormal staining in the ROI ranging from 0 to 100% (0 meaning normal; 100 meaning maximal pathology present throughout the whole ROI). The scores provided by the two scorers were averaged to produce a final score for each ROI in each rat. A similar procedure was used for NeuN staining, except that the severity score (0 to 10) this time represented loss of staining relative to the contralateral homologous ROI. Excellent interobserver reproducibility for this scoring procedure has been reported before.[10,21]

In addition, a 'weighted mean' SxA score for each rat was computed by averaging the ROI SxA values, weighted by their respective areas. To this end, for each rat the SxA score of each particular ROI was normalized for the ROI area, and these weighted scores were then averaged across all ROIs to obtain an area-weighted mean.

Note that visual scoring and automated cell counting for the OX42 dataset from the 45-minute tMCAo group was not performed *a priori* because both staining quality and slide mounting were suboptimal for most sections in all rats. This was a technical error unrelated to the presence of infarcts in this group.

The interrater correlation of SxA scores between the two independent raters across all data from all rats (both 45- and 15-minute tMCAo groups) was 0.97 and 0.96 for NeuN and OX42, respectively, Pearson's correlation coefficient: both $P < 0.01$ and not different from identity, indicating very strong reliability of this measure, similar to our previous finding.[10]

Software-Assisted Quantification of Cell Numbers

The procedure is illustrated in Figure 1. To automate image processing and analysis of a large number of ROIs using batch processing, each ROI of each section of each animal was saved as an individual image file using the batch command in Adobe Photoshop CS (Adobe Systems; see Figure 1B for illustration of the quantification process). After enhancing image contrast using the Auto Contrast command, noise reduction of grayscale images was achieved by consecutively using the Unsharp-Mask (amount 100%, radius 5 pixels, threshold none), Despeckle, and High-Pass filtering (radius 10 pixels) commands using Adobe Photoshop CS. Binarization of NeuN and OX42-stained images was performed using the ImageJ software Auto Threshold command (ImageJ, U.S. National Institutes of Health, Bethesda, MD, USA; http://imagej.nih.gov/ij/). For NeuN-stained images, the range of pixel intensity was then adjusted manually on an initial set of images to achieve optimal threshold values (i.e., optimal 'highlighting' of neuronal cell bodies). The determined range of pixel intensities was then used for automated thresholding of the remaining set of images. Similarly, for OX42-stained sections, the range of pixel intensities was first determined using the Auto Threshold command on an initial set of images, followed by subsequent manual adjustment to achieve optimal threshold values for subsequent automated processing. Of note, using OX42, an antibody against microglial integrin CD11b that is upregulated on activated microglia,[21] the differentiation between quiescent and activated microglia is based on differences in staining,[22,23] allowing for selective thresholding of activated microglia. Finally, the ImageJ Watershed algorithm was applied to both sets of NeuN and OX42-stained images to separate touching or overlapping cells. The total cell number for each ROI was automatically quantified using the Particle Analysis command. To allow for meaningful automated quantification of particles from binary image data (i.e., to avoid incorrect counting of 'background pixels' or 'giant particles') ranges of particle characteristics for automatic quantification were determined as follows: For NeuN-stained cells the average area and circularity of 300 cells from 10 randomly selected ipsi- and contralesional ROIs (30 cells per ROI) were assessed manually using the ImageJ Measure command. The average area and circularity of the selected NeuN-stained cells ±1 s.d. were subsequently used as inclusion ranges for automatic quantification. Similarly, using this method, ranges of particle characteristics for OX42-stained cells were determined on OX42-stained images. To match the metric used for the visual analysis, the relative change of the number of NeuN-stained neurons and OX42-stained microglia between corresponding ipsi- and contralesional ROIs was expressed for each ROI as a ratio of the number of NeuN/OX42-stained cells on the affected hemisphere/number of NeuN-/OX42-stained cells on the unaffected hemisphere. These cell counts normalized to the unaffected hemisphere will be referred to in what follows as 'NeuN ratios' and 'OX42 ratios', respectively. In addition, for each rat a whole-hemisphere average cell number change was calculated as the 'weighted mean' across all 44 ROIs, taking into account the area of each ROI. To this end, for each rat the NeuN or OX42 ratio for each particular ROI was normalized by the ROI area, and these normalized values then averaged across all ROIs to obtain an area-weighted mean for NeuN-stained neurons and for OX42-stained activated microglia, respectively.

Cell counting was feasible only when immunostained sections were of good or excellent quality. Exclusion was performed *a priori* by an external colleague masked to group assignment and unfamiliar with the purpose of this study. As a result, a number of sections were excluded *a priori* from the analysis (both methods). A particular case is rat 1 from the 45 minutes group in which several NeuN sections showed highly inconsistent staining and staining artefacts; accordingly, this rat was excluded from all subsequent analyses. Regarding the 28 days, 45 days, and 60 days survival subgroups from the 15 minutes group, 2/48 NeuN-stained and 4/48 OX42-stained; 3/24 NeuN-stained; and 6/24 NeuN-stained and 2/24 OX42-stained sections were excluded from subsequent analysis, respectively, resulting in an overall exclusion rate of 8.9%. Again, these exclusions were not related to the presence or extent of tissue damage.

Statistical Handling

Statistical analyses were performed using SPSS (version 15, SPSS, Chicago, USA) software. To assess whether individual ROIs showed significant changes in NeuN or OX42 SxA scores across all subjects from each group, the data for each ROI were tested against 0 using paired *t*-tests. To allow a meaningful comparison between the visual and cell counting methods, the same statistical test was applied to cell densities between ipsi- and contralesional sides. However, given their metrics were entirely different, the data derived from the two quantification methods were not directly compared. Nonparametric Kendall's tau was used to assess the correlation between visual scores and cell count ratios. Results were considered to be statistically significant if two-tailed $P < 0.05$.

RESULTS

45-Minute tMCAo Group

As explained above, only NeuN data were available for this set of rats. Based on visual analysis, both infarction and SNL were observed in 5/7 rats, rat 5 exhibited partial infarction in combination with SNL, and rat 3 had SNL only (see Ejaz *et al*[9] for details).

Table 1 shows the mean (± s.e.m.) weighted mean NeuN ratio and SxA score across the group.

Figures 2A and 2B, show the mean (± s.e.m.) SxA scores and NeuN ratios in the 44 ROIs, respectively. Across ROIs, the mean values ranged from zero (no change in any rat) up to nearly maximum (pan-necrosis in most rats), with the regional distribution of the changes being almost identical with the two methods. Affected ROIs were mostly located in the primary and secondary somatosensory areas, and to a lesser extent the insula, auditory, parietal and visual cortices. Assessing ROIs for statistically significant changes across the group, 13 and 19 ROIs were

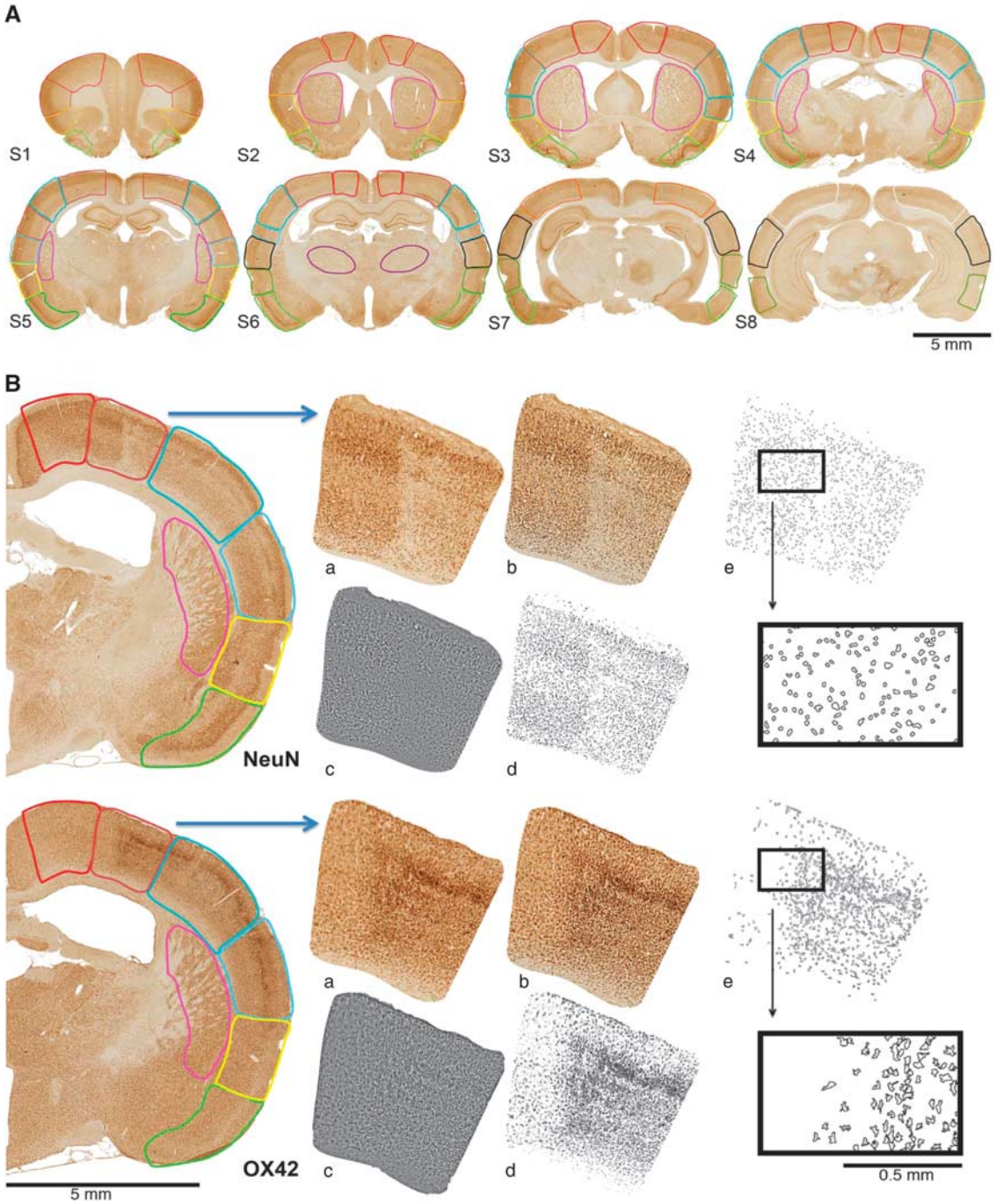

Figure 1. (**A**) Illustration of cytoarchitectonic ROI templates used for analysis shown on NeuN-stained whole-brain sections of a rat 60 days after 15-minute tMCAo, which were digitized using a Hamamatsu NanoZoomer slide scanner. Eight coronal sections, composed of 39 cortical, 4 caudate/putamen, and 1 thalamus ROI per hemisphere were selected for analysis (see Hughes *et al*, [10] for details). Lesion is on the right side of the scan. Scale bar, 1 mm. (**B**) Flow diagram exemplifying for one selected ROI (primary somatosensory cortex) with definite selective neuronal loss and colocalized microglial activation 28 days after 15-minute tMCAo, the software-assisted quantification of NeuN-stained and OX42-stained cells (upper and lower row, respectively; only the affected hemisphere is shown for illustration). Following manual application of the template each ROI was (a) processed as an individual image file using the batch command in Adobe Photoshop to (b) enhance contrast using the Auto Contrast command and (c) reduce background noise using Unsharp-Mask, Despeckle, and High-Pass filters. In (d), ImageJ batch processing was used to create binary images based on threshold values determined with the Auto Threshold command and (e) cell numbers were quantified based on average (±1 s.d.) value for size and circularity using the Particle Analysis command (see Materials and Methods section for details). In (e), outlines of the quantified particles are depicted; upper and lower inserts show small, round particles and larger, ramified particles representative of the characteristic shapes of neuronal cell bodies and activated microglia, respectively. See Materials and Methods for further details. ROI, region of interest.

individually significant using visual scoring and cell counting, respectively, again with essentially the same distribution with the two methods. Accordingly, there was an excellent correlation between mean SxA scores and NeuN ratios (Kendall's $\tau = -0.755$, $P < 0.001$, Figure 2C). Similarly significant correlations were present in all rats taken individually (data not shown).

15-Minute tMCAo Group

As expected, the ischemic changes after 15-minute tMCAo were much less prominent as compared with the 45 minutes tMCAo group, notably there was no instance of pan-necrosis. Based on the visual assessment, SNL was detected in 5/6, 2/3, and 2/3 rats at 28, 45, and 60 days post tMCAo, respectively. Corresponding MA was observed in 6/6, 1/3, and 1/3 rats at 28, 45, and 60 days post tMCAo, respectively (see Figure 1 for an illustrative example of colocalized cortical SNL and MA at 28 days post 15 minutes tMCAo). Table 1 shows the weighted mean (± s.e.m.) NeuN ratios, showing much lower values in the 28 days survival group than those found in the 45 minutes tMCAo group, as well as declining values with longer recovery times. This was also true for the OX42 ratios. This table also tabulates the SxA scores for NeuN and OX42, which showed changes parallel to but less sensitive than the corresponding ratios.

The spatial distribution of ischemic changes was similar to that observed with the 45 minutes tMCAo, i.e., the primary and secondary somatosensory areas including the barrel field were maximally affected, followed by the insula and parietal cortices (see Figure 1). These changes were of similar magnitude for NeuN and OX42, but again with much smaller values for both SxA and cell count ratios as compared with the 45-minute tMCAo group (data not shown). Like with the data shown in Table 1, the changes were more marked for the 28 days recovery group as compared with the 45 and 60 days groups, especially so for OX42. Accordingly, assessing individual ROIs for statistically significant local changes across the 28 days group ($n = 6$) and pooled 45 and 60 days ($n = 6$; for the sake of statistical power), there were 2 and 0 significant ROIs for SxA NeuN scoring; 9 and 8 for NeuN ratios; 18 and 0 for OX42 SxA scoring; and 15 and 3 for OX42 ratios, respectively.

There was high intermethod consistency for the 28-day recovery group (Kendall's $\tau = -0.569$ and 0.625 for NeuN and OX42, respectively; $P < 0.001$ for both; Figures 3A and 3B). Because of a loss of sensitivity of the visual method, the intermethod agreement for the 45-day recovery group was less strong yet still highly significant for OX42, but not significant anymore for NeuN (Kendall's $\tau = 0.419$ and -0.217; $P < 0.001$ and $P = 0.23$, respectively; Figures 3C and 3D). This disagreement was even worse for the 60 days recovery group, where there was no agreement at all with either immunostain (Figures 3E and 3F).

DISCUSSION

The aim of this study was to compare and assess the respective merits of two entirely different procedures designed to assess ischemic damage throughout the affected vascular territory after tMCAo in rodents, using the same objective ROI template applied to both protocols. One conspicuous strength of this study is that the two methods were evaluated within the same animals allowing for an optimal comparison.

To summarize the results, both methods produced similar findings in rats subjected to 45 minutes temporary distal tMCAo (Figure 2C), which induced mainly infarcts, as well as in rats subjected to 15-minute tMCAo producing pure SNL together with marked associated MA when assessed at 28 days postinjury (Figures 3A and 3B). However, as clearly depicted by Figures 3C–F, when assessing 15-minute tMCAo rats at later time points (45 and 60 days), the visual method picked up only the most marked changes but underestimated or missed completely the subtler cell changes, which were readily detected by the cell-counting method. This underestimation is also clear from Table 1, which shows the weighted mean cell changes across subjects in each group. Even accounting for the different metrics characterizing the two methods, both NeuN and OX42 SxA weighted mean scores were essentially zero at 45 and 60 days after 15-minute tMCAo (although significantly different from neutral for one of them), whereas the cell counting method did pick up sizeable and consistently significant changes. It would therefore appear from the present study that although the visual method is sensitive to even mild ischemic changes such as common degrees of SNL, it is poorly sensitive to more subtle changes such as mild/diffuse SNL or MA present late after the insult.

Previous studies have applied the visual method to a small set of prespecified brain regions or microscopic fields,[8,14,15] which is suboptimal when assessing tMCAo given the usually extensive ischemia as well as the intersubject variability in lesion topography. In our laboratory, Hughes *et al*[10] recently developed a similar approach but allowing for whole MCA territory assessment in a systematic and objective manner, by applying a template of ROIs derived from the stereotaxic atlas of the rat brain.[24] In the present study, we compared this validated method to the classical cell-counting method, for the first time adapting the latter so as to allow a similar whole MCA territory systematic assessment across the same ROI template as with the visual analysis to permit a direct comparison of the two methods. One potential advantage of the cell counting over the visual method is its more automated process, and hence anticipated reproducibility from laboratory to laboratory. This is the first study of its kind and there were no previous publication to compare our results to.

Apart from actual sensitivity, other factors need to be considered when assessing the relative merits of these two methods. Regarding the visual scoring method, standard immunohistochemical quality and image acquisition techniques are sufficient as assessment is performed at tissue level. In contrast, meticulous

Table 1. Weighted means (± s.e.m.) for ipsilateral/contralesional cell number ratios and visual SxA scores across rats for NeuN-stained sections at 28 days after 45-minute tMCAo ($n = 7$), and for both NeuN and OX42-stained sections obtained 28 days ($n = 6$), 45 days ($n = 3$), and 60 days ($n = 3$) after 15-minute tMCAo

	28 Days after 45-minute tMCAo	*28 Days after 15-minute tMCAo*	*45 Days after 15-minutes tMCAo*	*60 Days after 15-minute tMCAo*
NeuN ratio	$-23.4 \pm 5.1^{***}$	$-8.6 \pm 1.6\%^{***}$	$-5.5 \pm 1.1\%^{***}$	$-3.5 \pm 1.8\%^{*}$
NeuN SxA score	$12.0 \pm 3.0^{\#\#\#}$	$5.8 \pm 1.0^{\#\#\#}$	0.5 ± 0.3	$1.0 \pm 0.6^{\#\#}$
OX42 ratio	NA	$29.4 \pm 4.9\%^{***}$	$20.5 \pm 4.0\%^{***}$	$6.0 \pm 2.3\%^{*}$
OX42 SxA score	NA	$10.6 \pm 1.4^{\#\#\#}$	0.3 ± 0.2	0.1 ± 0.1

NA, not applicable; tMCAo, transient proximal middle cerebral artery occlusion. $^{*/***}P < 0.05/0.0001$ versus corresponding contralesional ROIs, paired *t*-test. $^{\#\#/\#\#\#}P < 0.01/0.0001$ paired *t*-test against neutral.

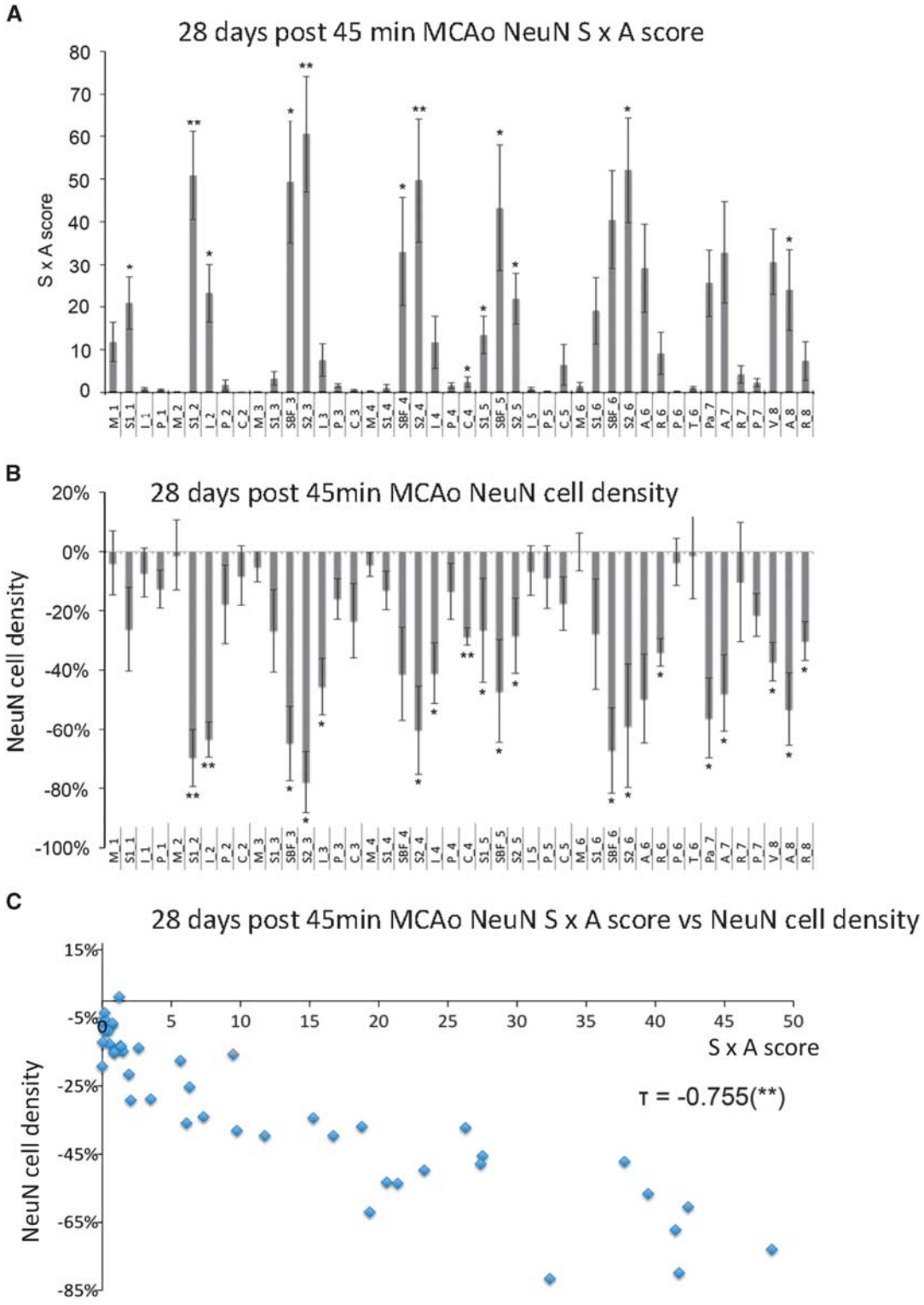

Figure 2. (**A**) Bar graph showing the mean (± s.e.m.) NeuN SxA scores for each of the 44 regions of interest (ROIs) at 28 days after 45-minute tMCAo across all animals ($n = 7$ rats per ROI; */**$P < 0.05/0.01$, paired *t*-test against 0). (**B**) Similarly laid out bar graph showing the mean (± s.e.m.) ipsilateral/contralesional NeuN cell number ratios for the 44 ROIs across all animals ($n = 7$ rats per ROI, */**$P < 0.05/0.01$ versus corresponding contralesional ROI, paired *t*-test). ROI code assignments: A, auditory cortex; C, caudate putamen; I, insular cortex; M, motor cortex; P, piriform cortex; Pa, parietal cortex; R, rhinal cortex; S1, primary somatosensory cortex; S2, secondary somatosensory cortex; SBF, primary somatosensory barrel field; T, thalamus; V, visual cortex (see Hughes *et al*,[10] for details). (**C**) Plot of NeuN SxA scores versus ipsilateral/contralesional cell number ratios for all 44 ROIs (mean values across seven animals, respectively), showing strong intermethod agreement ($\tau = -0.755$, $P < 0.001$).

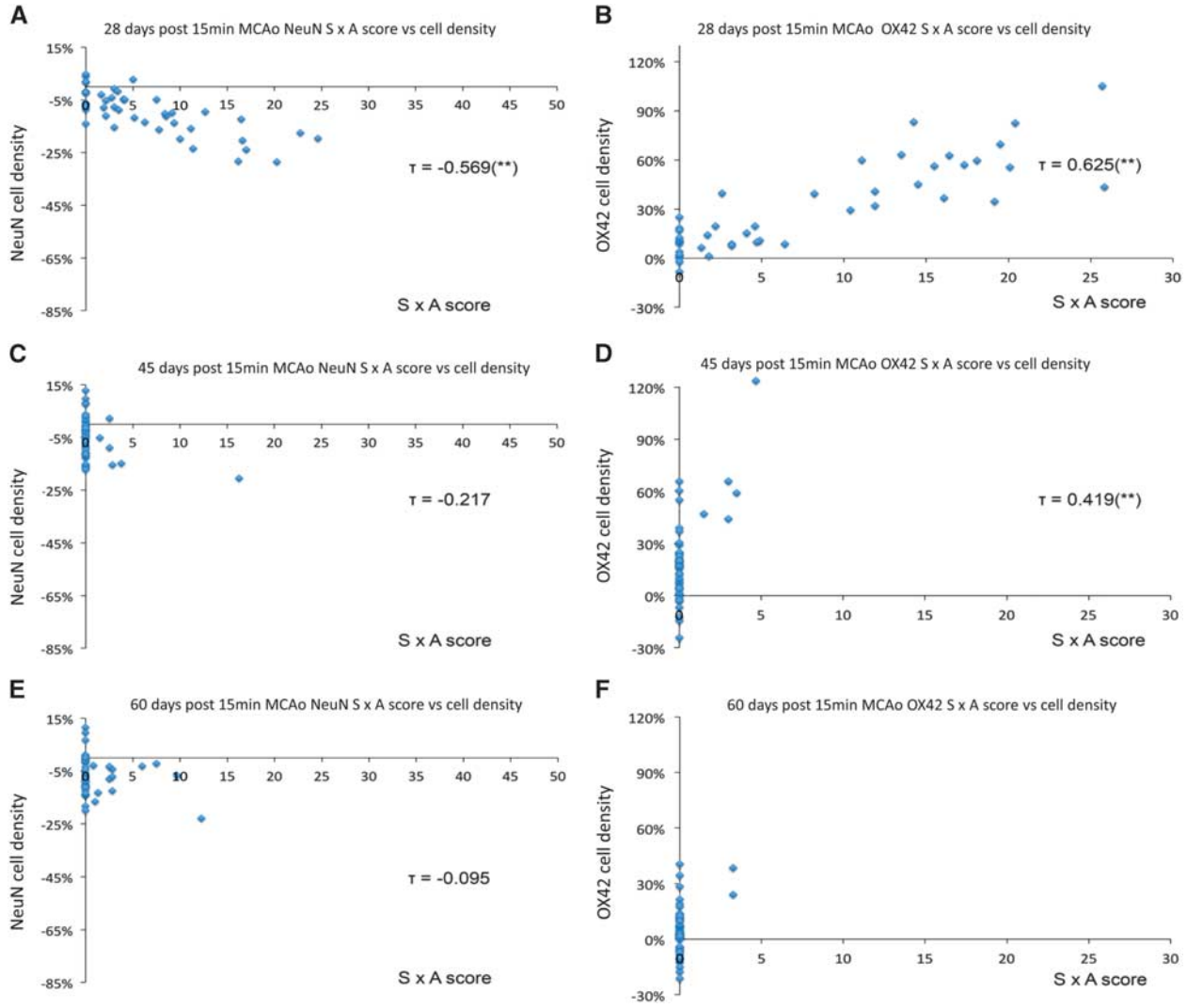

Figure 3. Plots of NeuN and OX42 SxA scores versus ipsilateral/contralesional cell number ratios for all 44 regions of interest (ROIs). Mean values across (**A** and **B**) six rats 28 days after 15-minute tMCAo showing strong intermethod agreement ($P < 0.001$ for both NeuN and OX42) for NeuN and OX42-stained cells, respectively, (**C** and **D**) three rats 45 days after 15-minute tMCAo showing significant intermethod agreement for OX42-stained cells ($P < 0.001$), but not for NeuN; and (**E** and **F**) three rats 60 days after 15-minute tMCAo, showing no intermethod agreement for either staining method.

tissue and immunohistochemical processing are required for the cell-counting method, as suboptimal quality (e.g., cutting artefacts, inconsistent staining, and damaged sections) will seriously hamper quantification accuracy. Regarding time efficiency, visual scoring allows for evaluation of MCA-territory pathology in ~30 minutes per brain, compared with ~90 minutes for scanning and evaluation using the cell counting method as used here. However, the visual evaluation requires raters experienced with the assessment of ischemia-induced brain histopathology and the scoring procedure, whereas ROI template application and particle quantification for the cell counting method can be performed by investigators without previous histopathologic experience. Assessment of ischemia-induced changes using the visual method is based on the underlying assumption that corresponding contralesional ROIs are intact. No such assumption is needed for the cell counting method which allows for within-subject comparison of absolute cell numbers between corresponding ipsi-/contralesional ROIs, resulting in strong statistical validity. Regarding equipment, the visual scoring can be performed using a conventional microscope camera and image processing software for ROI template application. In contrast, to efficiently process large number of sections using the cell counting method requires an automatic stage microscope or dedicated slide scanner and Adobe Photoshop (Adobe Systems) and ImageJ software for quantification. Table 2 summarizes the advantages and drawbacks of the two methods.

One important conclusion from our study is therefore that, given the above constraints of the cell-counting method, the visual method is acceptable as surrogate whenever visually evident damage such as infarction or substantial degrees of SNL and MA is considered. However, to quantify subtle, microscopic, damage requires the use of the former, in spite of it being more time consuming, cumbersome and expensive.

Limitations of our study include the relatively small sample size. However, the distal clip tMCAo method is skill-intensive, and the immunohistochemical processing time-consuming, so in practice only small samples can be assessed.[8–10,12] We chose here to assess cortical pathology because cortical SNL and MA are assumed to have particularly prominent behavioral consequences.[3,5–7,13] It would nevertheless be of interest to compare the visual scoring and cell-counting methods for striatal pathology as produced by proximal MCAo. We studied only spontaneously hypertensive rats

Table 2. Advantages and limitations of the two histology-based methods for whole-brain assessment of ischemic damage after tMCAo in rats assessed here

	Visual scoring	*Software-assisted cell counting*
Required quality of tissue processing and immunohistochemistry	Standard	Optimal
Required equipment	Standard	Expensive
Level of technical expertise required	High	Standard
Time efficiency	Good (~30 minutes per brain)	Poorer (~90 minutes per brain)
Quantitation	Semiquantitative	Fully quantitative
Sensitivity	Good for nonsubtle damage	Optimal even with subtle damage
Underlying assumption	Contralesional hemisphere intact	None
Assessment across the MCA territory	Yes	Yes

MCA , middle cerebral artery; tMCAo, transient proximal middle cerebral artery occlusion.

here because this is the strain that is most sensitive to ischemia and reflects a common clinical situation in ischemic stroke, namely chronic hypertension. However, it would be of interest to study other rat strains as well as mice. Finally, because of unexpected technical errors during immunohistochemical processing using OX42 antibody for the 45-minute tMCAo rats, we had to exclude all these sections from analysis. Note, however, that the expected less prominent MA present at 28 days after 15-minute tMCAo was readily picked up by both methods.

In conclusion, this is the first study to apply systematic assessment of postischemic SNL and MA across the MCA territory using both visual scoring and software-assisted cell counting methods. We show that both methods are adequately sensitive for the detection of damage including infarction and usual degrees of SNL and MA, and hence that the less cumbersome and expensive visual method can serve as a reliable surrogate for the cell counting method, including when staining quality is not optimal. Conversely, the latter is more reliable to pick up more subtle changes and should be implemented in such situations despite its more demanding staining and processing requirements.

DISCLOSURE/CONFLICT OF INTEREST

The authors declare no conflict of interest.

REFERENCES

1 Muir KW, Buchan A, von Kummer R, Rother J, Baron JC. Imaging of acute stroke. *Lancet Neurol* 2006; **5**: 755–768.
2 Astrup J, Siesjo BK, Symon L. Thresholds in cerebral ischemia—the ischemic penumbra. *Stroke* 1981; **12**: 723–725.
3 Baron JC, Yamauchi H, Fujioka M, Endres M. Selective neuronal loss in ischemic stroke and cerebrovascular disease. *J Cereb Blood Flow Metab* 2014; **34**: 2–18.
4 Baron JC. How healthy is the acutely reperfused ischemic penumbra?. *Cerebrovasc Dis* 2005; **20**: 25–31.
5 Wegener S, Weber R, Ramos-Cabrer P, Uhlenkueken U, Sprenger C, Wiedermann D *et al.* Temporal profile of T2-weighted MRI distinguishes between pannecrosis and selective neuronal death after transient focal cerebral ischemia in the rat. *J Cereb Blood Flow Metab* 2006; **26**: 38–47.
6 Wegener S, Weber R, Ramos-Cabrer P, Uhlenkueken U, Wiedermann D, Kandal K *et al.* Subcortical lesions after transient thread occlusion in the rat: T2-weighted magnetic resonance imaging findings without corresponding sensorimotor deficits. *J Magn Reson Imaging* 2005; **21**: 340–346.
7 Freret T, Bouet V, Leconte C, Roussel S, Chazalviel L, Divoux D *et al.* Behavioral deficits after distal focal cerebral ischemia in mice: usefulness of adhesive removal test. *Behav Neurosci* 2009; **123**: 224–230.
8 Qiao M, Zhao Z, Barber PA, Foniok T, Sun S, Tuor UI. Development of a model of recurrent stroke consisting of a mild transient stroke followed by a second moderate stroke in rats. *J Neurosci Methods* 2009; **184**: 244–250.
9 Ejaz S, Williamson DJ, Ahmed T, Sitnikov S, Hong YT, Sawiak SJ *et al.* Characterizing infarction and selective neuronal loss following temporary focal cerebral ischemia in the rat: a multi-modality imaging study. *Neurobiol Dis* 2013; **51**: 120–132.
10 Hughes JL, Beech JS, Jones PS, Wang D, Menon DK, Baron JC. Mapping selective neuronal loss and microglial activation in the salvaged neocortical penumbra in the rat. *Neuroimage* 2010; **49**: 19–31.
11 Garcia JH, Liu KF, Ye ZR, Gutierrez JA. Incomplete infarct and delayed neuronal death after transient middle cerebral artery occlusion in rats. *Stroke* 1997; **28**: 2303–2309. discussion 2310.
12 Katchanov J, Waeber C, Gertz K, Gietz A, Winter B, Bruck W *et al.* Selective neuronal vulnerability following mild focal brain ischemia in the mouse. *Brain Pathol* 2003; **13**: 452–464.
13 Sicard KM, Henninger N, Fisher M, Duong TQ, Ferris CF. Long-term changes of functional MRI-based brain function, behavioral status, and histopathology after transient focal cerebral ischemia in rats. *Stroke* 2006; **37**: 2593–2600.
14 Li F, Han SS, Tatlisumak T, Liu KF, Garcia JH, Sotak CH *et al.* Reversal of acute apparent diffusion coefficient abnormalities and delayed neuronal death following transient focal cerebral ischemia in rats. *Ann Neurol* 1999; **46**: 333–342.
15 Li F, Liu KF, Silva MD, Omae T, Sotak CH, Fenstermacher JD *et al.* Transient and permanent resolution of ischemic lesions on diffusion-weighted imaging after brief periods of focal ischemia in rats: correlation with histopathology. *Stroke* 2000; **31**: 946–954.
16 Ding G, Jiang Q, Li L, Zhang L, Zhang Z, Lu M *et al.* Longitudinal magnetic resonance imaging of sildenafil treatment of embolic stroke in aged rats. *Stroke* 2011; **42**: 3537–3541.
17 Weise G, Lorenz M, Posel C, Maria Riegelsberger U, Storbeck V, Kamprad M *et al.* Transplantation of cryopreserved human umbilical cord blood mononuclear cells does not induce sustained recovery after experimental stroke in spontaneously hypertensive rats. *J Cereb Blood Flow Metab* 2014; **34**: e1–e9.
18 Huttner HB, Bergmann O, Salehpour M, Racz A, Tatarishvili J, Lindgren E *et al.* The age and genomic integrity of neurons after cortical stroke in humans. *Nat Neurosci* 2014; **17**: 801–803.
19 Buchan AM, Xue D, Slivka A. A new model of temporary focal neocortical ischemia in the rat. *Stroke* 1992; **23**: 273–279.
20 Kaplan B, Brint S, Tanabe J, Jacewicz M, Wang XJ, Pulsinelli W. Temporal thresholds for neocortical infarction in rats subjected to reversible focal cerebral ischemia. *Stroke* 1991; **22**: 1032–1039.
21 Hughes JL, Jones PS, Beech JS, Wang D, Menon DK, Aigbirhio FI *et al.* A microPET study of the regional distribution of [11C]-PK11195 binding following temporary focal cerebral ischemia in the rat. Correlation with post mortem mapping of microglia activation. *Neuroimage* 2012; **59**: 2007–2016.
22 Kato H, Kogure K, Liu XH, Araki T, Itoyama Y. Progressive expression of immunomolecules on activated microglia and invading leukocytes following focal cerebral ischemia in the rat. *Brain Res* 1996; **734**: 203–212.
23 Schroeter M, Jander S, Huitinga I, Witte OW, Stoll G. Phagocytic response in photochemically induced infarction of rat cerebral cortex. The role of resident microglia. *Stroke* 1997; **28**: 382–386.
24 Paxinos G, Watson C. *The Rat Brain in Stereotaxic Coordinates*. Third edn. Academic Press: San Diego, London, 1996.